Electronic Supporting Information

Self-Division of Giant Vesicles Driven by an Internal Enzymatic Reaction

Ylenia Miele,[a] Zsófia Medveczky,[b] Gábor Holló,[c] Borbála Tegze,[d] Imre Derényi,[e] Zoltán Hórvölgyi,[d] Emiliano Altamura[f], István Lagzi,[b,c] Federico Rossi[a,f*]*

[a]Department of Chemistry and Biology "A. Zambelli" University of Salerno, Via Giovanni Paolo II 132, 84084 – Fisciano (SA), Italy

[b]Department of Physics, Budapest University of Technology and Economics H-1111, Budapest, Budafoki ut 8, Hungary

[c]MTA-BME Condensed Matter Research Group, Budapest University of Technology and Economics, H-1111, Budafoki út 8, Budapest, Hungary

[d]Department of Physical Chemistry and Materials Science, Budapest University of Technology and Economics, H-1111 Budafoki ut 8, Budapest, Hungary

[e]Department of Biological Physics, Eötvös Loránd University, H-1117 Pázmány Péter sétány 1/A, Budapest, Hungary

[f]Department of Chemistry, University of Bari, „Aldo Moro", Via Orabona 4, I-70125 Bari, Italy

[g]Department of Earth, Environmental and Physical Sciences – DEEP Sciences, University of Siena, Pian dei Mantellini 44, 53100 – Siena, Italy

1. Chemical model for the confined urea-urease enzymatic reaction

In the chemical model (Figure S4) we considered 7 main chemical species, namely urea (S, substrate), urease (E, enzyme), pyranine (fluorescent dye, pyrOH), oleic acid (HOA), acetic acid (HA), ammonia (NH_3) and carbon dioxide (CO_2). Some of these chemical species can be located outside of the vesicles having cross membrane properties. The transfer rates k_X (s^{-1}) are proportional to the vesicle surface/volume ratio and to the specific membrane permeability of each species:

$$k_X = \frac{3P_X}{R} \qquad (1)$$

where P_X (dm/s) is the permeability and R (dm) is the vesicle radius, respectively.

The rate of the enzyme-catalyzed reaction

$$CO(NH_2)_2 + H_2O \xrightarrow{urease} 2NH_3 + CO_2 \qquad (2)$$

is given by a modified Michaelis-Menten rate law, which accounts for the pH dependence and the product inhibition

$$R = \frac{v_{max}\,[S]}{\left(K_M + [S]\left(1+\frac{[S]}{K_S}\right)\left(1+\frac{[P]}{K_P}\right)\left(1+\frac{K_{es2}}{[H^+]}+\frac{[H^+]}{K_{es1}}\right)\right)} \qquad (3)$$

where $v_{max} = k_1[E]$, being [E] expressed as enzyme activity (units/mL), K_M is the Michaelis constant, K_{es1} and K_{es2} are protonation equilibrium constants of the substrate-enzyme complex, [P] is the concentration of the protonated form of ammonia (NH_4^+), [S] is the concentration of urea, K_S and K_P are the equilibrium constants for uncompetitive substrate and product inhibition, respectively.

The pH inside and outside the vesicles is governed by the following equilibria

$$\begin{aligned}
&NH_4^+ \overset{k_2}{\rightleftharpoons} NH_3 + H^+ && \text{rate} = k_2[NH_4^+] - k_{2r}[NH_3][H^+]\\
&CO_2 + H_2O \overset{k_3}{\rightleftharpoons} H^+ + HCO_3^- && \text{rate} = k_3[CO_2] - k_{3r}[HCO_3^-][H^+]\\
&HCO_3^- \overset{k_4}{\rightleftharpoons} CO_3^{2-} + H^+ && \text{rate} = k_4[HCO_3^-] - k_{4r}[CO_3^{2-}][H^+]\\
&H_2O \overset{k_5}{\rightleftharpoons} H^+ + OH^- && \text{rate} = k_5 - k_{5r}[OH^-][H^+]\\
&HA \overset{k_6}{\rightleftharpoons} A^- + H^+ && \text{rate} = k_6[HA] - k_{6r}[A^-][H^+]\\
&HOA \overset{k_7}{\rightleftharpoons} OA^- + H^+ && \text{rate} = k_7[HOA] - k_{7r}[OA^-][H^+]\\
&pyrOH \overset{k_8}{\rightleftharpoons} pyrO^- + H^+ && \text{rate} = k_8[pyrOH] - k_{8r}[pyrO^-][H^+]
\end{aligned} \qquad (4)$$

Finally, the transfer of the chemical species across the membranes can be considered as a first order process described by the following reactions

$$
\begin{aligned}
&\mathrm{S} \overset{k_S}{\rightleftarrows} \mathrm{S(out)} && \text{rate} = k_S\left([\mathrm{S}]-[\mathrm{S}]_o\right)\\
&\mathrm{NH_3} \overset{k_N}{\rightleftarrows} \mathrm{NH_3(out)} && \text{rate} = k_N\left([\mathrm{NH_3}]-[\mathrm{NH_3}]_o\right)\\
&\mathrm{CO_2} \overset{k_C}{\rightleftarrows} \mathrm{CO_2(out)} && \text{rate} = k_C\left([\mathrm{CO_2}]-[\mathrm{CO_2}]_o\right)\\
&\mathrm{HA} \overset{k_{HA}}{\rightleftarrows} \mathrm{HA(out)} && \text{rate} = k_{HA}\left([\mathrm{HA}]-[\mathrm{HA}]_o\right)
\end{aligned}
\qquad (5)
$$

where $[X]_o$ is the concentration of the chemical species of X outside the vesicles in the water phase.

The set of ordinary differential equations derived from the reaction rates (3) – (5) and reported in the main text in equations (1) and (2), was numerically integrated by using the software CO.PA.SI.[1,2] with the initial conditions and parameters listed in Table S1 and Table S2.

2. Molecular dynamics simulations

In the molecular dynamics (MD) simulations we used the Martini coarse-grained (CG) model to increase the length- and timescale compared to the all-atom simulations[3,4]. The force fields are available on the Martini web page: http://cgmartini.nl/. We used the MARTINI v2.2refP force field with the refined polarizable water model[5]. The model of oleate (OA^-) and oleic acid (HOA) was constructed according to Janke at *al.*[6] The simulations were performed with GROMACS 5.1.25[7]. VMD 1.9.3 was used in the visualization of the simulations results[8]. We set most of the parameters as denoted "New-RF" in de Jong et *al.*[9] and used 20 fs time step in the simulations with the dielectric constant of 2.5 because of the explicit screening of the polarizable water. The pressure was controlled with the Berendsen coupling method[10] (1.0 bar, semi-isotropic, τ_p = 5.0 ps) and the temperature was kept constant at 298 K. The bond constrains were maintained with the LINCS algorithm[11]. In the simulations, we examined the effect of the protonation–deprotonation on the structure of the POPC/HOA bilayer. The system contained 114,347 polarizable water, 2,080 POPC and 1,920 HOA molecules. According to the experiments, in the MD simulations only one leaflet of the bilayer was deprotonated. In the deprotonation, we exchanged HOA molecules with OA^- molecules and the closest water molecules to the head group of the OA^- with Na^+ ions to fulfill electroneutrality condition.

3. Film balance experiments

In the Wilhelmy film balance experiments, ethanol (Reanal), dichloromethane (Sigma-Aldrich), deionized water (18.2 MΩcm, purified with a Millipore Simplicity 185 filtration system) and buffer solutions were used. The buffer solutions were made with deionized water and given amounts (for pH values 6.0 and 7.0) of sodium phosphate monobasic dihydrate (Sigma-Aldrich) and sodium phosphate dibasic heptahydrate (Sigma-Aldrich).

A monolayer of molecules (POPC and HOA) was formed on a Teflon trough (laboratory-built Wilhelmy film balance, area and volume of 235 cm^2 and 800 cm^3, respectively) filled with an aqueous buffer solution. The surface pressure was measured with the Wilhelmy plate method. The surface pressure – area isotherms were measured at 26.0 ± 0.5 °C. Prior to the experiments, the trough was cleaned with ethanol, dichloromethane and deionized water, and then filled with the appropriate aqueous buffer solution (pH = 6.0 and 7.0). The liquid surface was cleaned of impurities by suctioning. In order to check the cleanliness of the interface, a surface pressure – area isotherm was measured, and if an increase (more than 1 mN/m) in the surface pressure was observed, the surface was cleaned and checked again. The concentration of the mixed solution of POPC and HOA in dichloromethane was 5 mM (2.6 mM for POPC and 2.4 mM for HOA). The appropriate amount of the solution (30 μl of a mixed solution of POPC and HOA) was spread drop by drop onto the liquid surface using a Hamilton syringe. After the solvent evaporation (10-15 min) the isotherm was measured by moving the barrier with a speed of 33 cm^2/min.

4. Description of videos

Video S1 shows the self-division process of a GUV triggered by a pH change generated by urea-urease enzymatic reaction.

Video S2 shows the self-division process and the increase of the fluorescent intensity inside the GUVs during the division.

Video S3 shows no division of GUVs by urea-urease enzymatic reaction in medium adjusted by a phosphate buffer (0.14 M, K_2HPO_4/KH_2PO_4).

Table S1. Initial concentrations and parameters used for the kinetic simulations. $[CO_2]$ and $[CO_2]_o$ are calculated by considering the solution at the equilibrium with the atmosphere at 25 °C; [HOA] + $[HOA]_o$ = 2 mM is the analytical concentration of oleic acid used for the vesicles preparation in experiments.

[X] (M)		Parameters	
[E] (U/mL)	1.1	N	10^4
[S]	0	R (dm)	5×10^{-5}
$[S]_o$	6×10^{-2}	V_i (dm^3)	5.24×10^{-13}
[pyrOH]	5×10^{-5}	V_o (dm^3)	3×10^{-5}
[HA]	1×10^{-6}	P_S (dm/s)[12]	4×10^{-7}
$[HA]_o$	1×10^{-6}	P_N (dm/s)[13]	1×10^{-3}
[HOA]	1×10^{-3}	P_{HA} (dm/s)[14]	6.5×10^{-4}
$[HOA]_o$	1×10^{-3}	P_C (dm/s)[15]	1.2
$[CO_2]$	1.2×10^{-5}		
$[CO_2]_o$	1.2×10^{-5}		

Table S2. Kinetic constants used in the model. Enzymatic constants were taken from refs.[16–19]; k_X were calculated from P_X and R reported in Extended Data Table 1; equilibrium rate constants were derived from the pK_a according to refs. [19–21].

Enzymatic		pH equilibria		
k_1 (u^{-1} mL M s^{-1})	3.7×10^{-6}		*forward* (s^{-1})	*reverse* (M^{-1} s^{-1})
K_m (M)	3×10^{-3}	k_2	24	4.3×10^{10}
K_{es1} (M)	5×10^{-6}	k_3	3.7×10^{-2}	7.9×10^4
K_{es2} (M)	2×10^{-9}	k_4	2.8	5×10^{10}
K_S (M)	3	k_5	1×10^{-3} (M^{-1} s^{-1})	1×10^{11}
K_P (M)	2×10^{-3}	k_6	7.8×10^5	4.5×10^{10}
		k_7	3.2×10^2	1×10^{10}
		k_8	1	2.5×10^7

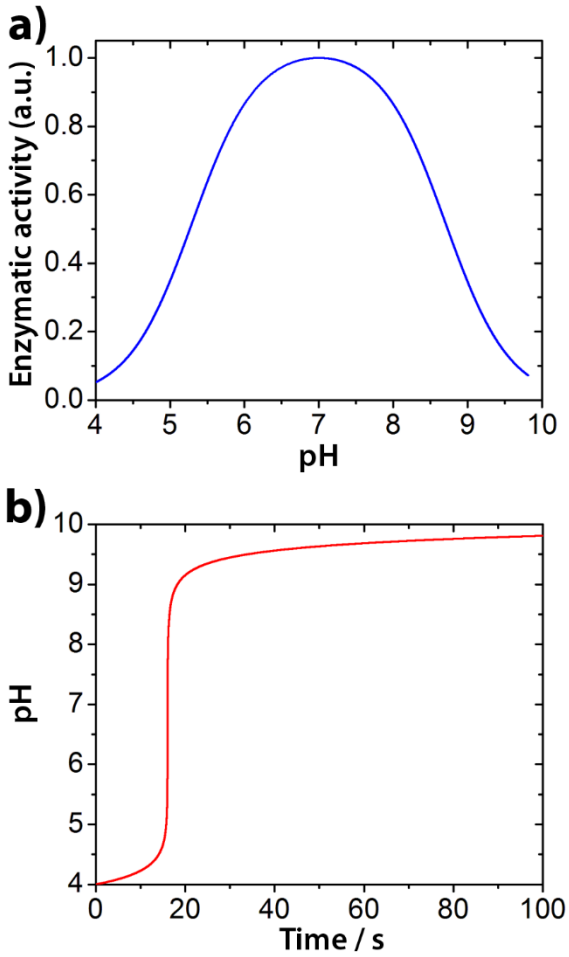

Figure S1. The characteristics of the urea-urease reaction. a) Dependence of the urea-urease reaction rate upon the pH in unbuffered solutions. b) autocatalytic profile of the pH during the urea-urease reaction.

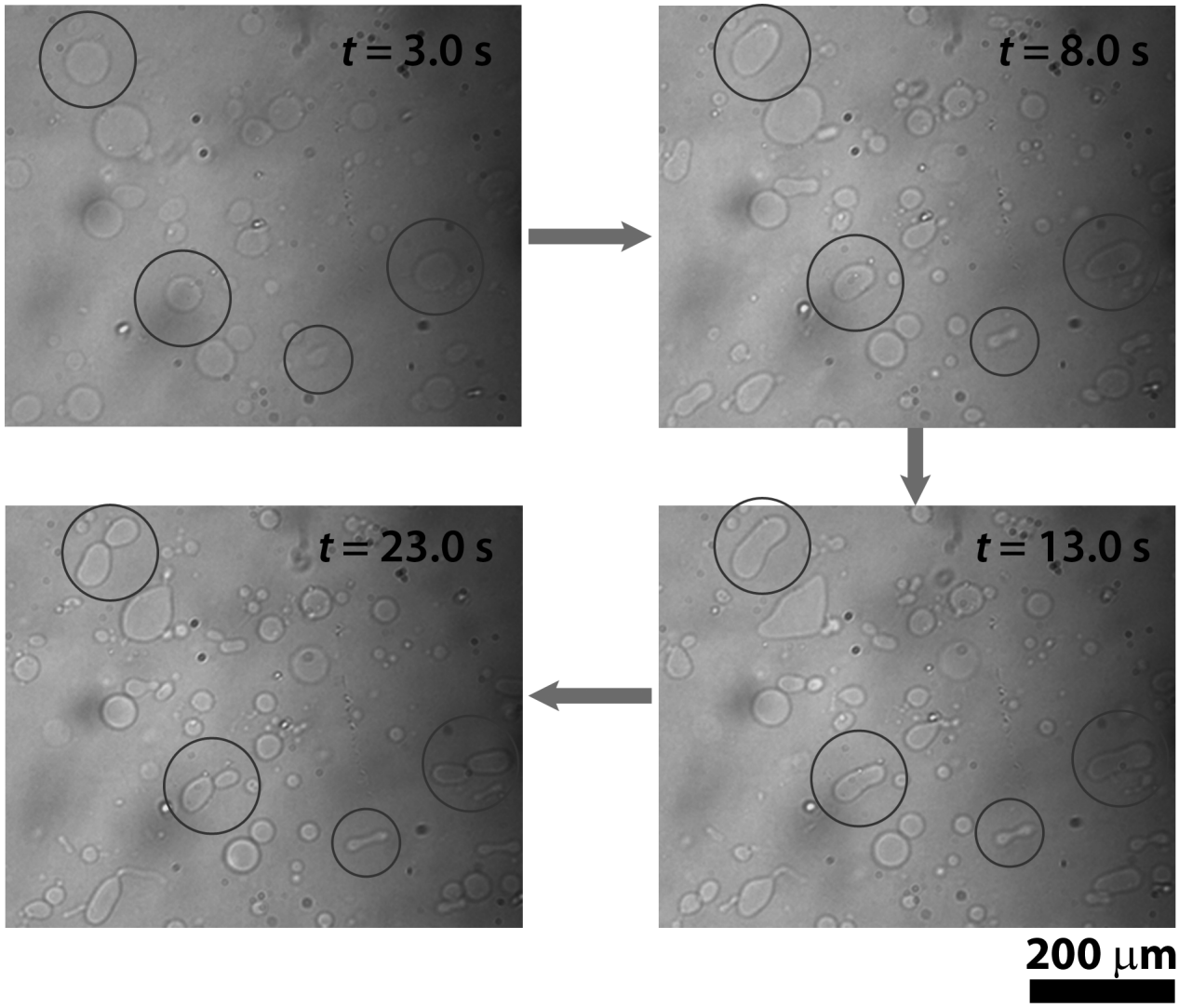

Figure S2. pH-triggered self-division of GUVs. Continuous shape transformation of a GUV, triggered by urea-urease enzymatic reaction, starting from a spherical shape through prolate and pear shapes into two daughter vesicles.

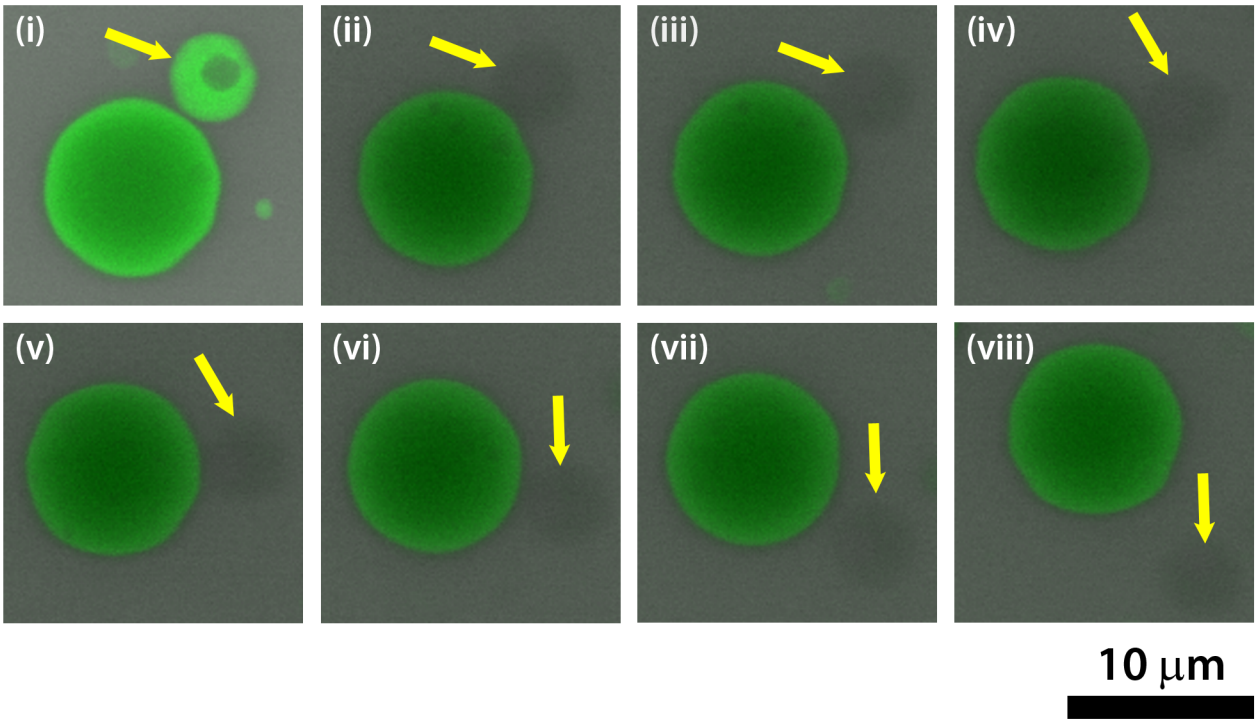

Figure S3. FRAP (fluorescence recovery after photobleaching) experiment using fluorescein as a fluorescent probe. The fluorescence of one of the two daughter vesicles (indicated by a yellow arrow) was bleached after the division process. The lack of fluorescence recovery indicates an effective separation between the two daughter vesicles. The initially clumped vesicles clearly separated after the irradiation with the laser beam. The time between consecutive fluorescence micrographs is 30 s.

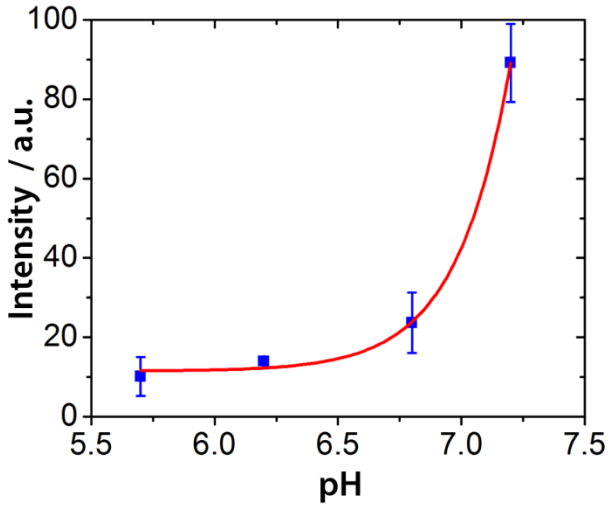

Figure S4. Calibration curve for pH. The calibration was performed by preparing a series of GUVs containing different buffers in the range of pH 5.5 and 7.5.

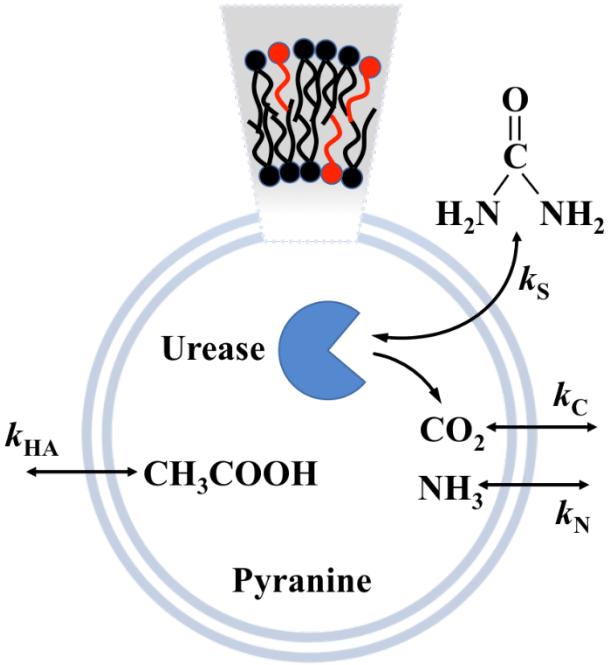

Figure S5. Sketch for the kinetic modeling of the system. All the chemical species that affect the pH are placed in the position at the beginning of the experiments. The black monomers in the double layer represent the inert POPC molecules; the red monomers represent oleic acid.

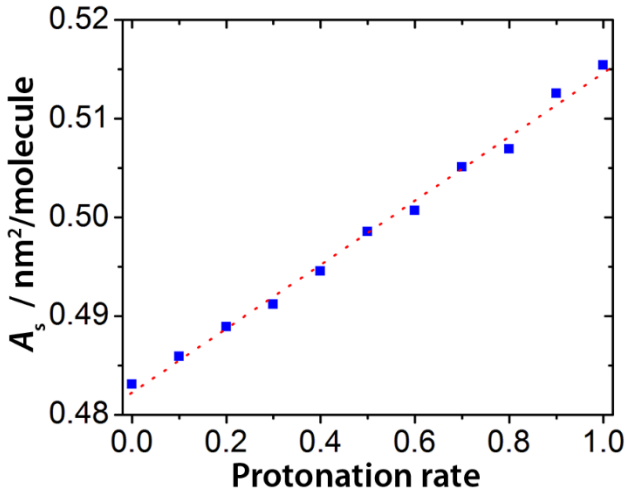

Figure S6. Results of the MD simulations. Effect of the protonation degree on the surface area of one leaflet of the mixed POPC/HOA bilayer in MD simulations.

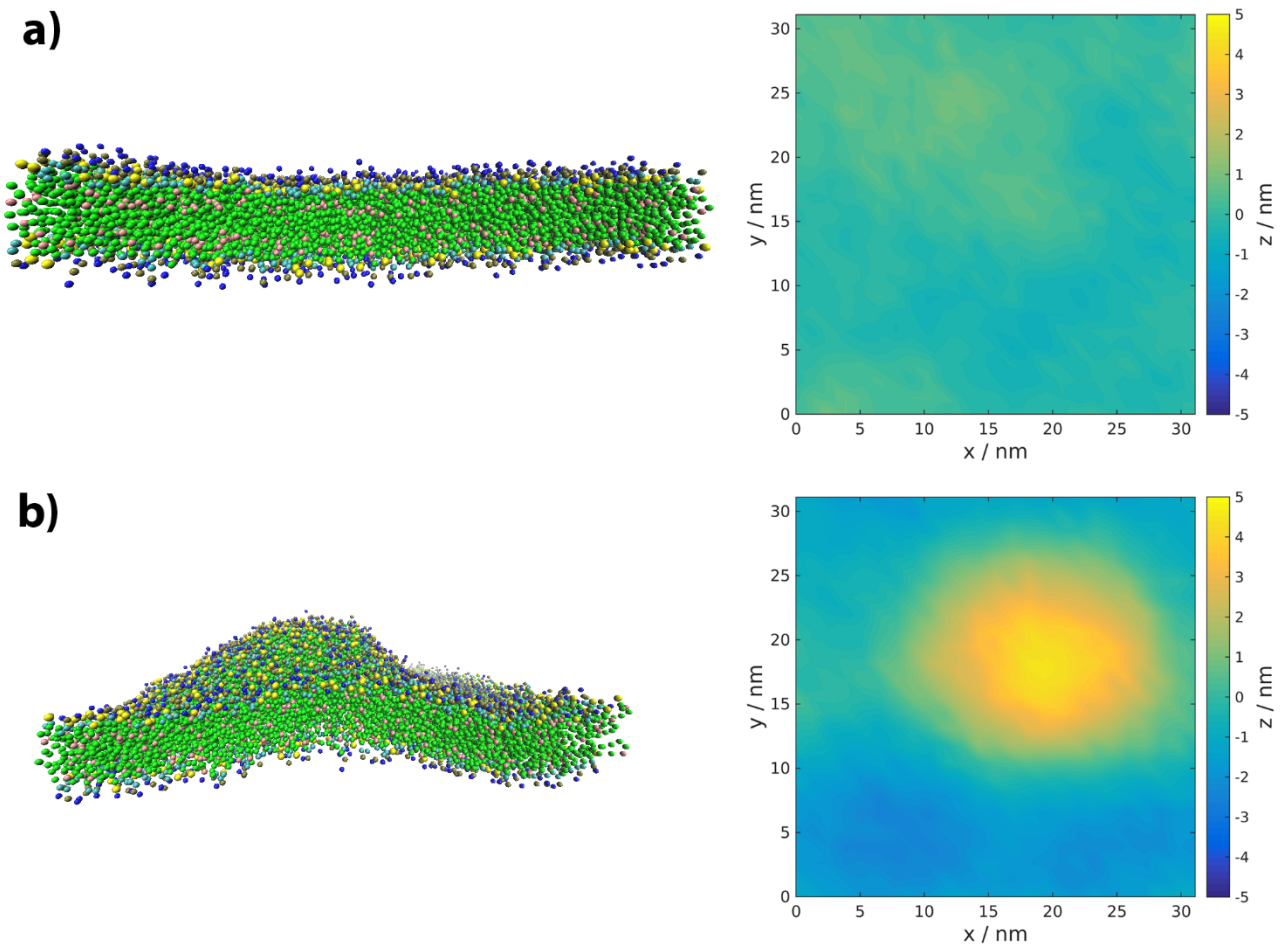

Figure S7. Results of the MD simulations. a) Structure of the mixed POPC/HOA bilayer, when all HOA molecules in the top leaflet are fully protonated (all HOA molecules have no charge). b) Structure of the mixed POPC/HOA bilayer, when all HOA molecules in the top leaflet are fully deprotonated (all HOA molecules have a negative charge).

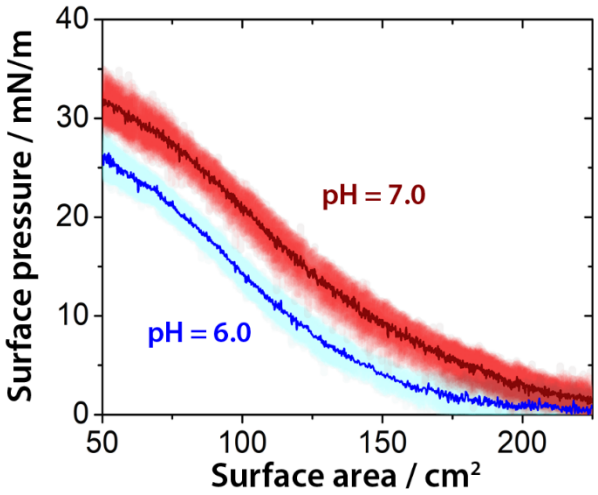

Figure S8. Surface pressure versus surface area isotherms of a monolayer of mixed POPC and HOA (2.6 mM:2.4 mM) using phosphate buffers at pH = 6.0 and 7.0. The solid line and the shaded area represent the average and the standard deviation of five independent experiments. Analyzing the isotherms the characteristics surface area was 150 ± 8 cm^2 and 174 ± 14 cm^2 at pH = 6.0 and pH = 7.0, respectively.

Supporting references

1 U. Kummer, S. Hoops, S. Sahle, R. Gauges, C. Lee, J. Pahle, N. Simus, M. Singhal, L. Xu and P. Mendes, *Bioinformatics*, 2006, **22**, 3067–3074.
2 CO.PA.SI. HomePage, http://www.copasi.org/tiki-index.php?page=homepage.
3 S. J. Marrink, A. H. de Vries and A. E. Mark, *J. Phys. Chem. B*, 2004, **108**, 750–760.
4 S. J. Marrink, H. J. Risselada, S. Yefimov, D. P. Tieleman and A. H. de Vries, *J. Phys. Chem. B*, 2007, **111**, 7812–7824.
5 J. Michalowsky, L. V. Schäfer, C. Holm and J. Smiatek, *J. Chem. Phys.*, 2017, **146**, 054501.
6 J. J. Janke, W. F. D. Bennett and D. P. Tieleman, *Langmuir*, 2014, **30**, 10661–10667.
7 M. J. Abraham, T. Murtola, R. Schulz, S. Páll, J. C. Smith, B. Hess and E. Lindahl, *SoftwareX*, 2015, **1–2**, 19–25.
8 W. Humphrey, A. Dalke and K. Schulten, *J. Mol. Graph.*, 1996, **14**, 33–38.
9 D. H. de Jong, S. Baoukina, H. I. Ingólfsson and S. J. Marrink, *Comput. Phys. Commun.*, 2016, **199**, 1–7.
10 H. J. C. Berendsen, J. P. M. Postma, W. F. van Gunsteren, A. DiNola and J. R. Haak, *J. Chem. Phys.*, 1984, **81**, 3684–3690.
11 B. Hess, H. Bekker, H. J. C. Berendsen and J. G. E. M. Fraaije, *J. Comput. Chem.*, 1997, **18**, 1463–1472.
12 A. Walter and J. Gutknecht, *J. Membrain Biol.*, 1986, **90**, 207–217.
13 M. B. Lande, J. M. Donovan and M. L. Zeidel, *J. Gen. Physiol*, 1995, **106**, 67–84.
14 T. X. Xiang and B. D. Anderson, *Biophys. J.*, 1997, **72**, 223–237.
15 A. Missner, P. Kügler, S. M. Saparov, K. Sommer, J. C. Mathai, M. L. Zeidel and P. Pohl, *J. Biol. Chem.*, 2008, **283**, 25340–25347.
16 M. Fidaleo and R. Lavecchia, *Chem. Biochem. Eng. Q.*, 2003, **17**, 311–318.
17 B. Krajewska and S. Ciurli, *Plant Physiol. Bioch.*, 2005, **43**, 651–658.
18 B. Krajewska, *J. Mol. Catal. B Enzym.*, 2009, **59**, 9–21.
19 G. Hu, J. A. Pojman, S. K. Scott, M. M. Wrobel and A. F. Taylor, *J. Phys. Chem. B*, 2010, **114**, 14059–14063.
20 M. Eigen, *Angew. Chem. Int. Ed.*, 1964, **3**, 1–19.
21 X. Wang, W. Conway, R. Burns, N. McCann and M. Maeder, *J. Phys. Chem. A*, 2010, **114**, 1734–1740.